The effects of magnesium oxide on the thermal, morphological, and crystallinity properties of metallocene linear low-density polyethylene/rubbers composite

Article · January 2013
DOI: 10.1515/polyeng-2013-0014

CITATIONS
4

READS
20

2 authors:

Ismaeel Alwaan
University Of Kufa
12 PUBLICATIONS **9** CITATIONS
SEE PROFILE

Azman Hassan
Universiti Teknologi Malaysia
271 PUBLICATIONS **3,246** CITATIONS
SEE PROFILE

DOI 10.1515/polyeng-2013-0014 — J Polym Eng 2013; 33(3): 229–238

Ismaeel M. Alwaan and Azman Hassan*

The effects of magnesium oxide on the thermal, morphological, and crystallinity properties of metallocene linear low-density polyethylene/rubbers composite

Abstract: The effects on the thermal, morphological, and crystallinity properties of the different loadings of magnesium oxide (MgO) blended with 10% rubbers [9:1 natural rubber (NR)/epoxidized NR] and metallocene linear low-density polyethylene (mLLDPE) in the presence of *N*,*N*-*m*-phenylenebismaleimide (HVA-2) compatibilizer were investigated. Fourier transform infrared spectroscopy showed that the epoxy and double-bond groups were absent in the blends. The crystallinity degree of mLLDPE composites were determined based on the results of differential scanning calorimetry. The crystallinity of the blends was continuously increased by the loading of MgO compared with blend of 0 phr MgO. Based on thermogravimetric analysis, the degradation temperature of NR in the blends with MgO is significantly enhanced compared with a pure NR and 0 phr MgO blend. The observations of the scanning electron micrographs indicate that the HVA-2 had caused a cross-linking reaction in the rubber phase and the domains of the MgO are separated from the continuous phase (mLLDPE).

Keywords: crystallization; metallocene linear low-density polyethylene (mLLDPE); morphology; natural rubber/epoxidized natural rubber (NR/ENR); thermal properties.

***Corresponding author: Azman Hassan,** Faculty of Chemical Engineering, Universiti Teknologi Malaysia, Johor Bahru, 8130, Malaysia, e-mail: azmanh@cheme.utm.my
Ismaeel M. Alwaan: Faculty of Chemical Engineering, Universiti Teknologi Malaysia, Johor Bahru, 8130, Malaysia; and Faculty of Engineering, University of Kufa, Najaf, Iraq

1 Introduction

Magnesium oxide (MgO) is used for wire and cable application and has been known to impart improved insulation properties for various applications [1]. Traditionally, additive agents and fillers are often used to improve the insulating and mechanical properties. In particular, several articles have reported that a nanocomposite of low-density polyethylene (LDPE) and MgO nanofillers shows superior characteristics as a candidate for future insulating material for DC power cables [2–5].

Thermal stability, flammability, and processability are important properties of wire and cable insulation materials. Linear low-density polyethylene (LLDPE) with excellent electrical properties, mechanical toughness, good resistance to chemicals, and ease of processing has been used as an insulation material for several applications [6, 7]. However, its applications are restricted due to its flammability and poor thermal properties. Flame inhibition can be performed on a physical basis as addition of inert fillers ($MgOH_2$, MgO), as heat sinks, or the release of inert gases (H_2O, CO_2, NH_3) [8, 9].

The incorporation of magnesium hydroxide ($MgOH_2$) into silane cross-linked LLDPE results in improved flame retardation, whereas limiting oxygen index, time to ignition, and the residue after combustion increase as the $MgOH_2$ content increases [10]. Thermal analysis techniques [thermogravimetric analysis (TGA), differential scanning calorimetry (DSC), differential thermal analysis (DTA) etc.] have been most important in the characterization of the flame-retardant features and the thermal stability of polymers and in the study of retardation of the mechanism [11].

The metallocene linear low-density polyethylene (mLLDPE) from single-site-constrained geometry catalysts optimizes polymer chain architecture to generate highly uniform polymer molecules with specific target properties. This technology of molecular synthesis and molecular control for polyolefin provides new options for replacing or modifying materials across a broad spectrum of processes and applications [6]. Wang et al. [12] reported that the amount of space charge accumulated in the developed polyethylene (PE) polymerized using the metallocene catalyst is smaller than that of conventional PE. Taniguchi et al. [13] studied the space charge behavior in LDPE polymerized using a metallocene catalyst. The experimental results revealed that the space charge amounts decreased when film density increased.

Blending polymers is a common technology frequently applied to develop a product with superior mechanical properties from an inexpensive polymer material and small amounts of compatibilizers [14]. Epoxidized natural rubber (ENR-50) was used as a compatibilizer for different blends [15–17]. *N*,*N*-*m*-Phenylenebismaleimide (HVA-2) was also shown to be an effective compatibilizer by reducing the interfacial tension and improving the adhesion between immiscible polymers [18–20].

In addition, it is also essential to study the morphology of blends to gain insight into the resistance of the material to crack growth failure. The resultant preparation of polymer blend depends on the proportion and properties of the individual polymeric components and the mode of dispersion and interaction between the phases. Homogeneity at the microscopic level is necessary to optimize the performance behavior of the polymer blends [21, 22].

The thermal degradation and crystallization behavior of polymer blends are very critical in assessing their processing property relationship [23, 24]. The physicomechanical and thermal properties of these blends are dependent on the crystallinity developed and on their morphological properties. Hence, the morphology of the blends depends on the molding condition and the relative crystallization time and temperature [25, 26].

This present study investigates mLLDPE filled with 9:1 natural rubber (NR)/ENR blend. NR has been chosen as one of the blend constituents for its good electrical characteristics. The other blend constituent, chosen because of its reasonably good impact strength and good solvent and oil-resistance properties and is an effective compatibilizer, is ENR containing 50 mol% of epoxy groups. MgO, besides its excellent dielectric properties, also acts as a flame-retardant and thermal polymer stabilizer. In addition, 2 phr HVA-2 was used as a compatibilizer for all compounds. Therefore, the objective of this article is to investigate the thermal stability, morphological, and crystallization properties of mLLDPE/(NR/ENR-50) (90:9:1 wt%) blend at different contents of MgO (5–20 phr) to assess the suitability of these blends for engineering applications and, in particular, to determine if this blend delivers a better performance than unmodified mLLDPE.

2 Experimental

2.1 Materials

The mLLDPE polymer matrix Exceed 1018CA was obtained from ExxonMobil Chemical Singapore Pte. Ltd. It has a density of 0.918 g/cm^3, a melt flow index of 1.0 g/10 min, and a DSC melting peak at 119°C [27]. The second component was NR (SMR-L grade) obtained from the Rubber Research Institute of Malaysia. The third component used in this study, ENR with 50 mol% epoxidation (grade EPOXYPRENE 50), which has a specific gravity of 1.03 and a Mooney viscosity, M_L, of 140 at a temperature of 100°C, was obtained from the Malaysian Rubber Board, Malaysia. The compatibilizer used for the blend was HVA-2, a free radical cross-linking agent from DuPont Dow Elastomers. The physical properties of HVA-2 are a melting point of 195°C and a density of 1.44 g/cm^3.

Magnesium Oxide Grade EMAG® 1000, a calcined natural MgO manufactured by Queensland Magnesia's Pty. Ltd., Australia, is mined from a high-quality cryptocrystalline magnesite deposit [28]. EMAG® 1000 is a nontoxic, pale pink powder. It is characterized by a high magnesium content and neutralizing property. The chemical analysis and physical properties are given in Table 1.

2.2 Preparation of blends

Initially, all raw materials were dried in an oven at 80°C for 24 h before processing. Compositions consisting of HVA-2 were mixed separately with rubber to obtain a homogenous mix using a milling machine (Double Elephant Brand SWX, China). This uniformly mixed compound was manually shredded to pieces using a pair of scissors. The pellets were compounded with mLLDPE and MgO using a twin screw extruder (Brabender PL2000, Germany, with L/D=30 and D=2.5 cm) at a barrel temperature of 140°C, 145°C, and 150°C at the feeding, metering, and die zones, respectively, at a speed of 45 rpm. The prepared compound was mixed in a milling machine at 110°C to obtain a homogenous mixture. Test samples were prepared by compression molding (Guthrie Industries Malaysia Shd. Bhd., RPM 0014-02-60T, Malaysia) at 205°C and under 70 kg/cm^2 of pressure for 15 min. The percentage of rubber

Table 1 Chemical analysis and physical properties of magnesium oxide grade EMAG® 1000 [12].

Chemical analysis (%)		Physical properties	
MgO	94.0	Specific surface area	38 m^2/g
SiO_2	2.4	Loose fill density	700 kg/m^3
CaO	3.0	Sizing	500 μm
Al_2O_3	0.20		
Fe_2O_3	0.26		
Mn_3O_4	0.14		

content of NR/ENR-50 was fixed at 90/10 wt%. The compound formulations are given in Table 2.

2.3 Differential scanning calorimetry

The thermal properties of mLLDPE, NR, ENR-50, and their blends were determined using a differential scanning calorimeter DSC7 (Perkin-Elmer, USA). Samples are analyzed by DSC over the temperature range ambient to 200°C. A heating rate of 10°C/min and a nitrogen atmosphere flow rate of 20 ml/min were used. The temperature was kept at 50°C and 200°C for 5 min before heating and cooling at the same rate to study the thermal history. The melting temperatures of the samples, T_m, were taken as the endothermic peaks of the thermograms, whereas the fusion heats, ΔH_f, were calculated as the areas under endothermic peaks.

The percentage of crystallinity was calculated as the enthalpy of fusion taken from DSC test divided by the enthalpy of 100% crystalline PE. The latter was taken as 279 J/g [29, 30]. The crystallinity (xc %) was calculated according to Eq. (1):

$$xc\ \% = \frac{\Delta H_f}{k\Delta H_o} \quad (1)$$

where ΔH_f is the melting enthalpy of the sample, ΔH_o is the melting enthalpy of 100% crystalline PE, and k is the weight percent of the mLLDPE in blends.

2.4 Thermogravimetry analysis

TGA is usually used to measure the amount and rate of change in the mass of a material as a function of temperature or time. TGA was carried out with a TGA7 thermogravimetric (Perkin-Elmer, USA) analyzer. The samples were heated from room temperature to 900°C in a 20-ml/min flow of N_2 at a scanning rate of 10°C/min. The mass loss of each sample was measured as a function of temperature at a given heating rate.

Table 2 mLLDPE/NR/ENR/MgO/HVA-2 compound formulations.

Materials	Designations					
	A1	A2	B1	B2	B3	B4
mLLDPE[a]	100	90	90	90	90	90
Rubber (90% NR+10% ENR)[a]	0	10	10	10	10	10
Magnesium oxide[b]	0	0	5	10	15	20
HVA-2[b]	0	2	2	2	2	2

[a]Weight percent.
[b]Parts per hundred parts (phr) of total polymer (rubber and mLLDPE).

2.5 Fourier transform infrared spectroscopy

Fourier transform infrared spectroscopic (FTIR) analysis (Perkin-Elmer, USA) was used to study the chemical structures of mLLDPE, NR, ENR-50, MgO, and their composites. The infrared sample spectrum was conducted using a Perkin-Elmer FTIR spectrophotometer. The measurements were done over a range of 4000–370 cm^{-1} at room temperature, and a uniform resolution of 16 cm^{-1} was maintained in all cases.

2.6 Morphological analysis

The studies were performed using a scanning electron microscope (SEM) model JEOL JSM-6390 LV, USA on the liquid nitrogen-fractured surfaces and benzene-extracted samples with 1 KX magnifications. Samples were coated with thin layer of gold before examination under the electron beam, and an operating voltage of 15 kV was used.

3 Results and discussion

3.1 FTIR spectroscopy

The FTIR spectrum of ENR and NR is presented in Figure 1. The characteristic bands observed: 2963.28 and 2960.99 cm^{-1} (–C–H aliphatic stretching), 1450.07 and 1448.6 cm^{-1} ($–CH_2–$ bend), 1378.23 and 1375.92 cm^{-1} ($–CH_3$ symmetric bending), 701.09 and 737.88 cm^{-1} [$–(CH_2)_n–$ wagging], respectively. The band stretching of the –C=C band of the ENR and NR was observed at 1662 cm^{-1}, and the unsaturated group (>C–CH–) appeared in NR spectrum at 836.33 cm^{-1}. The epoxide group of ENR-50 (C–O–C) showed in the FTIR spectrum at 1250.56 and at 875.48 cm^{-1}. This result was similar to the observation by Latif et al. [31].

Figure 1 presents the FTIR spectrum of the mLLDPE (A1): 2918.7 cm^{-1} (–C–H aliphatic stretching), 1465.27 cm^{-1} ($–CH_2$ bend), weak peak at 1371.76 cm^{-1} ($–CH_3$ symmetric bending) due to the presence of hexane side chain, and 719.47 cm^{-1} [$–(CH_2)_2–$ wagging] due to the presence of PE chain. These results are in agreement with the work of Saha et al. [32] and Sedlarik et al. [33].

The MgO curve shows a broad absorption with the absorption peak of 3435 cm^{-1}, which is the characteristic stretching vibration of hydroxylate (–OH). Peaks localized

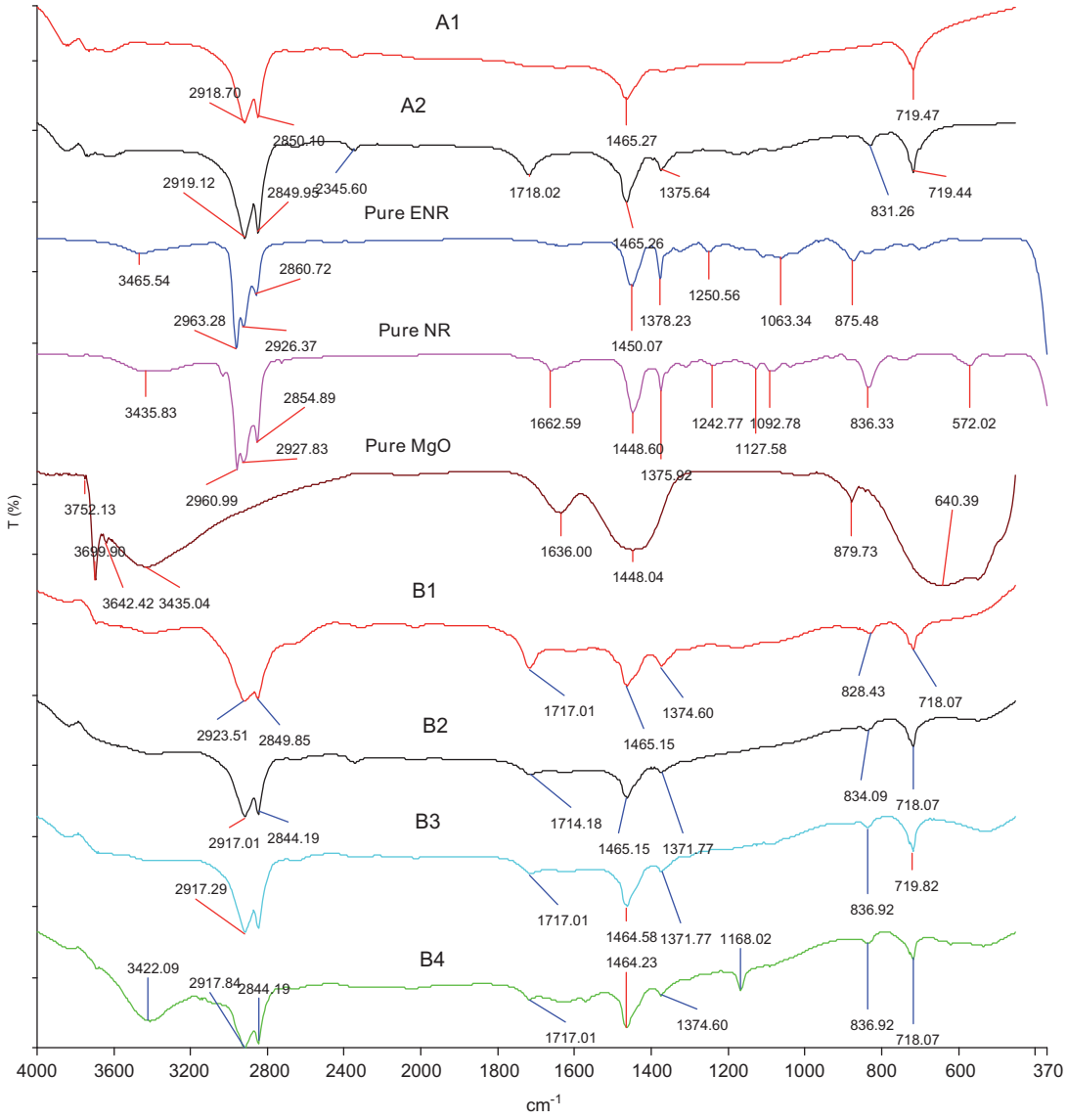

Figure 1 FTIR results for pure mLLDPE (A1), ENR-50, NR, and A2, B1, B2, B3, and B4 blends.

at 1636 cm^{-1} are assigned to the asymmetrical vibration of carboxylate (O–C=O). A characteristic band of nitrate ions at 1448 cm^{-1} is observed from the FTIR spectra. The absorption bands at 879.73 cm^{-1} are attributed to the characteristic absorption peaks of cubic MgO. The absorption bands of the NO_3 group at 640.39 cm^{-1} are shown in Figure 1 on the MgO curve. The groups of –OH, O–C=O, and NO_3^- may be used in the raw materials' structure to prepare MgO.

The FTIR spectrum of A2, B1, B2, B3, and B4 composites are presented in Figure 1: 2919–2923 cm^{-1} (–C–H aliphatic stretching), 1465 cm^{-1} ($-CH_2$ rocking), 1375.64–1371.77 cm^{-1} ($-CH_3$ symmetric bending), and 719 cm^{-1} [$-(CH_2)_n-$ wagging]. A band at 828–838 cm^{-1} was due to the epoxide group of ENR-50 (C–O–C).

Meanwhile, the C–O–C and C=C bands of the ENR-50 at 1250.56 and 1660 cm^{-1}, respectively, were found to be absent in all blends. Therefore, it can be assumed that the opening of the double bond in NR and ENR-50 may be due to the formation of an interchain cross-link in the system. However, the –C=O band appeared at 1718 cm^{-1} in all compounds and the B1 blend has a stronger band than others. Moreover, in the B4 blend, it was observed that –OH group appeared at band 3422.1.

In the rubber industry, MgO is used as an activator, and its role in the mechanism of accelerated sulfur vulcanization has been studied [34, 35]. It was clear from the FTIR that the MgO loading and the –C=O band at 1718 cm^{-1} has an inverse relationship, i.e., an increase in the concentration of MgO in the blends will result in

a decrease in the concentration of –C=O group in the blends, as revealed by a continuously reducing intensity of –C=O peak [36] with increased MgO loading. It may be concluded that MgO worked as an activator for HVA-2 to change the reaction mechanism by reducing the concentration of the –C=O group in the blends. Therefore, it is possible that the B1 blend has a stronger band than others because the loading of the 5-phr MgO was insufficient in bringing about a reduction in the concentration of the carbonyl group by the HVA-2.

The –OH group in the B4 blend represents the alcoholic (OH) group because the C–O group appeared near 1300–1000 cm^{-1} [37] (in our case, 1168 cm^{-1}). It is possible that increasing the concentration of the activator (MgO) up to 20 phr causes a new reaction mechanism in the B4 blend to produce –OH alcoholic group, where such behavior of materials reaction is related to catalyst concentration [38].

3.2 Effect of MgO on the crystallization of mLLDPE/10% rubber

The thermal and crystallization behaviors of the virgin mLLDPE and 10% rubber/mLLDPE with and without MgO (5–20 phr) blends with the compatibilizer HVA-2 under nonisothermal conditions have been studied using DSC. The crystallinity of the A2 blend was reduced from a neat polymer and shows the largest reduction compared with all other blends, as shown in Figure 2. The reduction in the degree of crystallinity indicates an interference in the form of NR molecular incorporation into the LLDPE part [39]. Dahlan et al. [39] suggested that these interactions are in the form of physical cross-links between the amorphous parts of NR and LLDPE and that compatibility is created by the interfacial penetration between the separated phases of the blends. Therefore, in blend A2, the physical cross-links increased to the point that more cross-links appeared in this blend than any other.

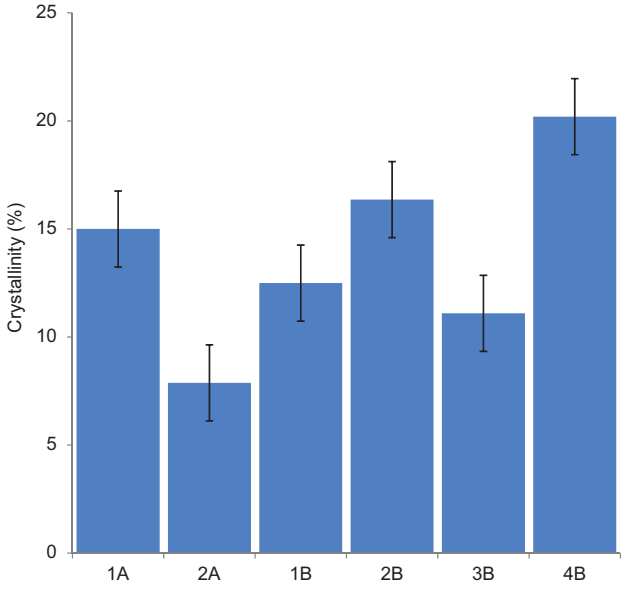

Figure 2 Crystallinity of pure mLLDPE (A1) and A2, B1, B2, B3, and B4 blends.

The reduction of the crystallinity of mLLDPE in the A2 blend compared with a neat mLLDPE may be due to an increase in the chemical cross-linking density by rubber loading to the mLLDPE. A similar observation was also reported by Moly et al. [40]. They studied the crystallization of the LLDPE/EVA blends with and without dicumyl peroxide as the cross-linking agent. They found that the increase in cross-linkings was caused by decreasing crystallinity. Inoue and Suzuki [41] investigated the effects of the cross-linking of ethylene-propylenediene terpolymer (EPDM) particles in the polypropylene (PP) matrix on crystallinity behavior. They also found that an increased cross-linking of the EPDM caused a decrease in the crystallinity of PP. The decrease in crystallinity as a result of cross-linking is due to the fact that cross-linking hinders the ordered arrangement of the polymer chains [40].

Meanwhile, as shown in Figure 2, the crystallinity of B1 and B3 blends was reduced from a neat polymer, respectively, therefore the physical cross-links of B1 and B3 blends would increase. Moreover, the crystallinity of B2 and B4 blends increased from a virgin polymer (mLLDPE), and the maximum crystallinity was observed in B4 blend. As a result, the interfacial adhesion and interaction between the stress concentrate zones in the mLLDPE matrix for both of blends decreased [39, 42].

Furthermore, the increase of the crystallization in B2 and B4 composites was attributed to the heterogeneous nucleation of MgO in the blends. When the crystallinity of the B1, B2, B3, and B4 blends were compared with the A2 blend without MgO, it was found that the crystallinity increased with an increase of MgO loading, as shown in Figure 2. This result can be explained by the heterogeneous nucleation of MgO in the blends. Therefore, the interfacial adhesion and interaction between the stress concentrate zones in the mLLDPE matrix for all blends decreased with the increase in MgO loading [39, 42].

Similar results were obtained by many researchers. Ning et al. [43] studied the effect of whisker (SiO_2–MgO–CaO) nucleation ability on the interfacial crystal morphology of PE/whiskers composites. They found that the nucleation ability of the whiskers leads to a denser high density polyethylene (HDPE) and that the crystal lamellae grew on the

surface of the whisker. Gao et al. [44] studied crystalline structures, especially the interfacial crystalline layers of semicrystalline polymer PP/whisker composites. They adopted two drawn ratios and observed that the shish-calabash structure was obtained at the low drawn ratio and the transcrystalline structure was obtained at the high drawn ratio. Ning et al. [45] found that the interfacial crystalline morphology has been successfully obtained in the injection-molded bar of the iPP/SiO_2–MgO–CaO (SMCW) whisker composites and LLDPE/SMCW composites.

The crystallinity of the mLLDPE suddenly decreased at the B3 blend compared with the B1, B2, and B4 blends. This phenomenon is attributed to two competing factors: cross-link density and nucleation of MgO filler. The increasing cross-linking of rubbers caused a decrease in the crystallinity of mLLDPE [40]. Meanwhile, the heterogeneous nucleation of MgO in the blends would result in an increase in the crystallinity of the mLLDPE [43]. Thereby, the interaction of the cross-link density and nucleation of MgO filler contributes to the varied percent crystallinity of the mLLDPE composites. Therefore, it can be concluded that, compared with all other blends, the lower crystallinity at the A2 blend can be attributed to the cancellation of one of the factors affecting the increase in crystallinity, which is the nucleation of MgO filler, and the remaining cross-linking density factor, which causes a decrease in crystallinity.

Table 3 reveals the results of onset (T_{onset}), end (T_{end}), and peak (T_{peak}) temperatures of pure mLLDPE and the A2, B1, B2, B3 and B4 blends. The results show that they were constant with different blends, except that the T_{onset} of the B1 blend was slightly lower than the A2 blend. Therefore, the loadings of MgO between 5 and 20 phr have no effect on the onset, end, and peak temperatures of mLLDPE in the blends.

The percentage of crystallinity was calculated as the enthalpy of fusion taken from the DSC test divided by the enthalpy of 100% crystalline PE. The results, as shown in Figure 2, indicate that the A2 blend has the lowest percentage of crystallinity followed by the B1, B2, and B4 blends, respectively. It should be noted that the crystallinity of the B3 blend has the same value as the B1 blend.

Table 3 Effect of different loading of MgO on T_{onset}, T_{end}, and T_{peak} of the pure mLLDPE (A1) and the A2, B1, B2, B3, and B4 blends.

Composition	T_{onset} (°C)	T_{end} (°C)	T_{peak} (°C)
A1	104.79	120.80	115.17
A2	107.32	120.12	114.97
B1	104.38	120.05	114.87
B2	106.01	120.26	115.10
B3	107.55	120.30	114.73
B4	106.49	120.62	114.70

3.3 Thermogravimetric analysis

The TGA and DTG curves of samples are presented in Figure 3A–H. It shows that pure mLLDPE, NR, and ENR-50 depict a single step of degradation (Figure 3A–C) during the thermal degradation process. The maximum (T_{max}) and 5 wt% ($T_{5\%}$) decomposition temperatures of pure mLLDPE were higher than both pure NR and pure ENR-50, with no residue remaining, as shown in Table 4, whereas the NR has a lower degradation temperature at both maximum (T_{max}) and 5 wt% ($T_{5\%}$) decomposition temperatures (Table 4), indicating poor thermal stability. Both the ENR-50 and NR show no residue remaining. It is suggested that the degradation of pure mLLDPE in nitrogen is mainly due to the decomposition of macromolecular, with a complex radical chain mechanism, including initiation reactions, propagation reactions, and termination reactions. Table 4 shows the degradation temperature at 5 wt% ($T_{5\%}$), the maximum temperature (T_{max}) of the first peak, the start degradation temperature (T_s), and T_{max} of second peak for pure and composites materials.

The decomposition behavior of the A2 blend is shown in Figure 3D. There was no overlapping region between the mLLDPE and the rubber. The mLLDPE began to decompose after the decomposition of rubber was completed. The thermal degradation of the A2 blend was shown in two steps. From the degradation of the pure mLLDPE and two types of pure rubber, it can be concluded that the first step would correspond to the rubber decomposition and the second step would correspond to mLLDPE degradation. It was noted from Table 4 that the degradation temperature of NR in the blend is significantly higher than that of pure NR, suggesting that the presence of mLLDPE delayed the decomposition of NR and presented one peak of rubber revealing a good compatibility between the two rubbers (NR/ENR-50); therefore, the thermal stability of NR is improved. Another possible reason that the thermal stability of the A2 blend improved may be the cross-linking of the unsaturated part of the rubber phase, thereby resulting in chain stiffening and improved thermal stability [23]. The reason that the presence of the cross-linked network structure causes a higher thermal stability of the cross-linked blends is the number of bonds per unit mass of polymer, which is increased after cross-linking. Although the degradation process of the A2 blend started at a high temperature, the addition of rubbers shifted the

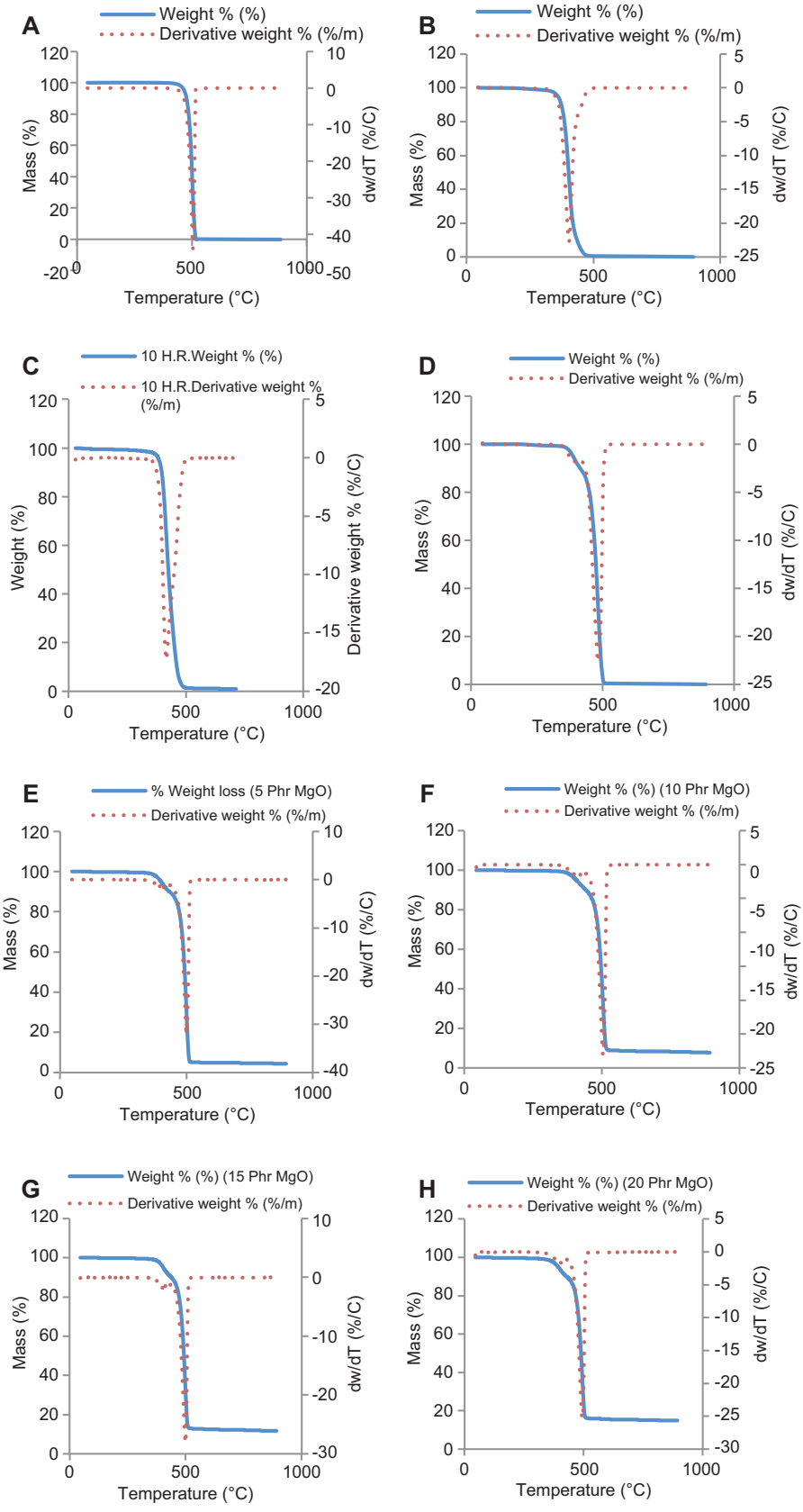

Figure 3 The TGA and DTG curves of pure (A) mLLDPE, (B) NR, and (C) ENR-50 and blend of (D) A2, (E) B1, (F) B2, (G) B3, and (H) B4, at a heating rate of 10°C/min in an N_2 atmosphere.

Table 4 Degradation temperature at 5 wt% ($T_{5\%}$), maximum temperature (T_{max}), and start degradation temperature (T_s) for mLLDPE, NR, ENR, and their composites.

Materials and composition	First peak		Second peak	
	$T_{5\%}$	T_{max}	T_s	T_{max}
Pure NR	359.51	401.42		
Pure ENR-2	385.73	418.1		
A1	466.41	505.1		
A2	387.01	388.8	408.8	482.8
B1	399.671	401.131	431.131	500.131
B2	407.58	419.45	425.45	504.45
B3	403.62	411.938	434.938	498.938
B4	393.25	405.54	423.54	494.54

degradation temperature and maximum temperature of the mLLDPE (second step) to lower temperatures than pure mLLDPE as shown in Table 4.

The maximum (T_{max}) and 5 wt% ($T_{5\%}$) decomposition temperatures of the B1, B2, B3, B4 blends are shown in Figure 3E–H and Table 4. There was no overlapping region between the mLLDPE and rubber. The thermal degradation of the B1, B2, B3, and B4 blends were shown in two steps. From the degradation of pure mLLDPE and the two types of pure rubber, it can be concluded that the first step would correspond to rubber decomposition and the second step would correspond to mLLDPE degradation. It is noted that the degradation temperature of NR in the blends with MgO is significantly higher than that of pure NR and A2 blend without MgO, suggesting that the presence of MgO delayed the decomposition of NR in blends because it forms a nonvolatile char barrier that minimizes the diffusion of oxygen to the polymer substrate and also reduces heat transfer from the heat source to the polymer substrate [46]. The presence of one peak for rubber decomposition reveals a good compatibilization between the two rubbers (NR/ENR-50); therefore, the thermal stability of NR is improved in blends with MgO.

Another reason for the increase in the thermal stability of the B1, B2, B3, and B4 blends can be explained in terms of the crystallinity and morphology of the blends. It is known that the crystalline materials are more stable than the amorphous materials due to a higher energy required to overcome both strong intramolecular and intermolecular forces [23]. It was observed that the crystallinity of the B1, B2, B3, and B4 blends increased with an increase in MgO loading compared with the A2 blend without MgO, as shown in Figure 2, resulting in the increased thermal stability of the B1, B2, B3, and B4 blends. An additional reason may be that there is a possibility that the cross-linking of the unsaturated part of the rubber phase causes improved thermal stability [23].

The addition of MgO shifted the start degradation temperature and maximum temperatures of the B1, B2, B3, and B4 blends (second step) to slightly lower temperatures than pure mLLDPE, as shown in Table 4. Meanwhile, the start degradation temperature of the mLLDPE (second step) in the B3 blend was higher than other blends with MgO. Therefore, the B3 blend was more thermally stable than the other blends with MgO composites. This behavior may be attributed to the B3 blend having a higher cross-linking density than other blends, and this result was in agreement with the crystallinity result that a high cross-linking of the B3 blend causes a crystallinity reduction in the B3 blend. Meanwhile, the maximum degradation temperature of mLLDPE (second step) in the blends with MgO remained nearly constant at 500°C.

3.4 Morphological studies

The resultant properties of polymer blends depend on the proportion and properties of the individual polymeric components and the mode of dispersion and interaction between the phases. The homogeneity at the microscopic level is necessary for the optimum performance behavior of the polymer blends. It is essential to study the morphology of the polymer blends to assess the homogeneity of mixing and the compatibility of the polymeric components involved.

The electron micrographs of the liquid nitrogen-fractured surfaces of the blends, after the extraction of the NR/ENR-50 phase with benzene, are shown in Figure 4A–D. The scanning electron micrographs of the A2 blend without MgO are presented in Figure 4B. In the case of the A2 blend, rubber is in a dispersed phase and mLLDPE is in continuous phase, and these are demonstrated in Figure 4B. In these micrographs, there are no voids as the dark phases are formed by the extracted rubber by benzene solvent. This observation indicates that HVA-2 had caused a cross-linking reaction in the rubber phase and increased the interfacial adhesion resulting from the formation of graft copolymer [20]. Another possible reason for the disappearance of voids is shown in SEM micrographs (in Figure 4B), in which the small NR and ENR-50 composite particles have fully dissolved in the mLLDPE matrix due to the increase in interfacial adhesion. The morphology of the liquid nitrogen-fractured surfaces of pure mLLDPE homopolymer is shown in Figure 4A, which clearly shows, as expected, that no voids are present.

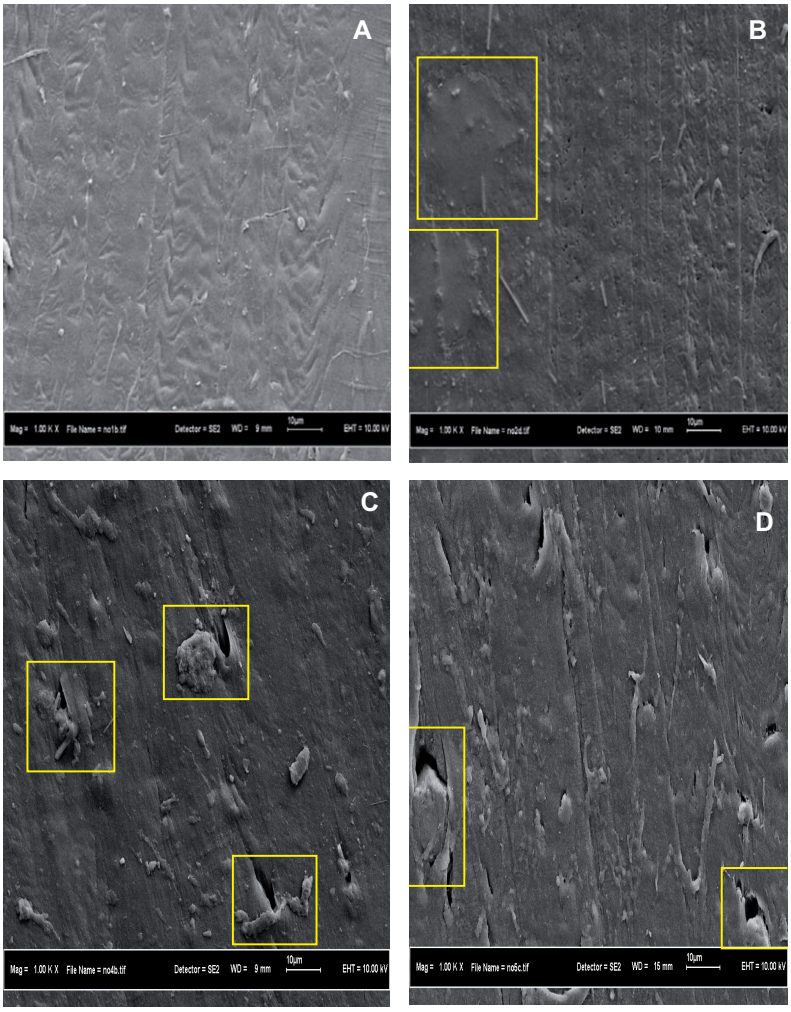

Figure 4 SEM micrographs of the liquid nitrogen-fractured surfaces. (A) Pure mLLDPE, (B) A2 blend, (C) B1 blend, and (D) B4 blend.

Figure 4C and D shows the MgO-filled A2 blend at the 5- and 20-phr loading of MgO. It can be clearly seen that the domains of the MgO are separated from the continuous phase (rubber/mLLDPE). The polarity of the MgO filler is obviously not capable of forming a good filler-matrix interaction with the non-polar mLLDPE blends because mLLDPE has little affinity for MgO filler due to large surface energy differences.

4 Conclusion

The effects of MgO loadings on the thermal, crystallinity, and morphological properties of mLLDPE/NR/ENR-50 blends with HVA-2 compatibilizer have been investigated. FTIR revealed that the HVA-2 caused cross-linking in the blends by opening the double bond and epoxy groups. The MgO plays a role in the heterogeneous nucleation of the blends and causes a decrease in the interfacial adhesion and interaction between the stress concentrate zones in the mLLDPE matrix. The loadings of MgO between 5 and 20 phr have no effect on onset, end, and peak temperatures of mLLDPE in the blends. Pure NR has a lower thermal stability than pure ENR-50 and mLLDPE. The presence of MgO delayed the decomposition of NR in blends, and a higher thermal stability was observed in the B3 blend than other blends. A good compatibilization was obtained between the two rubbers (NR/ENR-50) in all blends using HVA-2. The scanning electron micrographs of the A2, B1, B2, B3, and B4 blends revealed that the HVA-2 had caused a cross-linking reaction in the rubber phase and the domains of the MgO are separated from the continuous phase.

Received January 15, 2013; accepted March 7, 2013; previously published online April 6, 2013

References

[1] Andritsch T, Kochetov R, Morshuis PHF, Smit JJ. International Conference on Solid Dielectrics, Potsdam, Germany, July 4–9, 2010.

[2] Murata Y, Sekiguchi Y, Inoue Y, Kanaoka M. ISEIM 2005, Proceedings of the 2005 International Symposium on Electrical Insulating Materials, June 5–9, 2005, vol. 3, pp. 650–653.

[3] Takada T, Hayase Y, Tanaka Y. *IEEE Trans. Dielect. Electr. Insul.* 2008, 15, 152–160.

[4] Murakami Y, Nemoto M, Okuzumi S, Masuda S, Nagao S, Hozumi N, Sekiguchi Y. *IEEE Trans. Dielect. Electr. Insul.* 2008, 15, 33–39.

[5] Ishimoto K, Kanegae E, Ohki Y, Tanaka T, Sekiguchi Y, Murata Y, Reddy C. *IEEE Trans. Dielect. Electr. Insul.* 2009, 16, 1735–1742.

[6] Han SJ, Gross LH. Electrical Insulation Conference and Electrical Manufacturing Expo, October 22–24, 2007, pp. 80–84.

[7] Müller M, Kulikov O, Hornung K, Wagner MH. *Polym. Sci. Ser. A* 2010, 52, 1163–1170.

[8] Take A. *Polym. Degrad. Stab.* 1991, 33, 171–206.

[9] Jiao C, Wang Z, Chen X, Yu B, Hu Y. *Radiat. Phys. Chem.* 2006, 75, 557–563.

[10] Wang Z, Hu Y, Gui Z, Zong R. *Polym. Test.* 2003, 22, 533–538.

[11] Jianqi W, Darning F, Wenhui W, Minxiu Z, Yi L. *Polym. Degrad. Stab.* 1991, 31, 129–140.

[12] Wang S, Fujita M, Tanimoto G, Ajda F, Fujiwara Y. Conference Record of the 1996 IEEE International Symposium on Electrical Insulation, Montreal, Quebec, Canada, June 16–19, 1996, vol. 2, pp. 657–660.

[13] Taniguchi Y, Kaneko K, Mizutani T, Ishioka M. ISEIM 2001, Proceedings of 2001 International Symposium on Electrical Insulating Materials, 2001, pp. 440–443.

[14] Zurina M, Ismail H, Ratnam CT. *Polym. Test.* 2008, 27, 480–490.

[15] Guo B, Cao Y, Jia D, Qiu Q. *Macromol. Mater. Eng.* 2004, 289, 360–367.

[16] Noriman NZ, Ismail H, Rashid AA. *Polym. Test.* 2010, 29, 200–208.

[17] Poh BT, Ismail H, Tan KS. *Polym. Test.* 2002, 21, 801–806.

[18] Awang M, Ismail H. *Polym. Test.* 2008, 27, 321–329.

[19] Jayasree TK, Predeep P, Thomas S, Laladas KP. *J. Polym. Mater.* 2003, 20, 227–236.

[20] Hassan A, Wahit MU, Chee CY. *Polym. Test.* 2003, 22, 281–290.

[21] Ghosh P, Chattopadhyay B, Sen AK. *Polymers* 1994, 35, 3958–3965.

[22] Gaylord NG. *J. Macromol. Sci. Chem. A.* 1989, 26, 1211–1229.

[23] Najib NN, Ismail H, Azura AR. *Polym. – Plast. Technol. Eng.* 2009, 48, 1062.

[24] Hemmati M, Narimani A, Shariatpanahi H, Fereidoon A, Ahangari MG. *Int. J. Polym. Mater.* 2011, 60, 384.

[25] Rajalekshm S, Joseph R. *Int. J. Polym. Mater.* 2005, 54, 917.

[26] John N, Singh S. *Int. J. Polym. Mater.* 2011, 60, 255.

[27] ExxonMobil Chemical. *Metallocene Polyethylene Resin Exceed 1018CA*, 2011. Available at: www.exxonmobilpe.com. Accessed on January 1, 2012.

[28] Queensland Magnesia. *Magnesium Oxide Grade EMAG® 1000*. Available at: http://www.qmag.com.au/pdf/EMAG1000.pdf. Accessed on January 2, 2012.

[29] Wang X, He HQ, Tu DM, Lei C, Du QG. *IEEE Trans. Dielect. Electr. Insul.* 2008, 15, 319–326.

[30] Ferreto HFR, Oliveira ACF, Lima LFCP, Parra DF, Lugao AB. *Radiat. Phys. Chem.* 2012, 81, 958–961.

[31] Latif F, Aziz M, Katun N, Ali AMM, Yahya MZ. *J. Power Sources* 2006, 159, 1401–1404.

[32] Saha N, Zatloukal M, Saha P. *Polym. Adv. Technol.* 2003, 14, 854–860.

[33] Sedlarik V, Saha N, Saha P. *Polym. Degrad. Stab.* 2006, 91, 2039–2045.

[34] Guzmán M, Vega B, Agulló N, Giese U, Borrós S. *Rubber Chem. Technol.* 2012, 85, 38–55.

[35] Chokanandsombat Y, Sirisinha C. *J. Appl. Polym. Sci.* 2013, 128, 2533–2540.

[36] Pretsch E, Buhlmann P, Badertscher M. Structure Determination of Organic Compounds Tables of Spectral Data. 4th ed., Berlin: Springer-Verlag, 2009.

[37] Pavia DL, Lampman GM, Kriz GS. Introduction to Spectroscopy: a Guide For Students of Organic Chemistry. 3rd ed., USA: Thomson Learning, Inc., 2003.

[38] Papaspyrides CD, Kampouris EM. *Polymers* 1986, 27, 1437–1440.

[39] Dahlan HM, Zaman MDK, Ibrahim A. *Polym. Test.* 2002, 21, 905–911.

[40] Moly KA, Radusch HJ, Androsh R, Bhagawan SS, Thomas S. *Eur. Polym. J.* 2005, 41, 1410–1419.

[41] Inoue T, Suzuki T. *J. Appl. Polym. Sci.* 1995, 56, 1113–1125.

[42] Wang Z, Qu B, Fan W, Hu Y, Shen X. *Polym. Degrad. Stab.* 2002, 76, 123–128.

[43] Ning N, Deng H, Luo F, Wang K, Zhang Q, Chen F, Fu Q. *Composites B* 2011, 42, 631–637.

[44] Gao Y, Ren K, Ning N, Fu Q, Wang K, Zhang Q. *Polymers* 2012, 53, 2792–2801.

[45] Ning N, Fu S, Zhang W, Chen F, Wang K, Deng H, Zhang Q, Fu Q. *Progr. Polym. Sci.* 2012, 37, 1425–1455.

[46] Tesoro GC. *J. Polym. Sci. Macromol. Rev.* 1978, 13, 283–353.